scientific reports

Check for updates

OPEN

Multi-omics analysis of *Trichoderma reesei* mutant with high glucanase activity

Na Wang[1,2,3], Qing Lin[1,2], Zihan Wang[1,2], Honglin Shi[1,2], Yan Gao[1,2], Jun Zen[1,2], Kai Lou[1,2]✉ & Xiangdong Huo[1,2]✉

Trichoderma reesei **is one of the most important industrial filamentous fungi that produce large amounts of extracellular enzymes. β-Glucanase is used widely in biofuels, food, and animal feed. Here, a higher β-glucanase activity mutant was obtained from *T. reesei* via atmospheric and room temperature plasma (ARTP) mutagenesis. Compared with that of the original strain, the β-glucanase activity of the mutant ARTP-9 increased by 56.23%, reaching 45.12 U/mL and its enzymatic activity demonstrated transgenerational stability. Compared with the original strain, transcriptome sequencing revealed 1793 differentially expressed genes (DEGs), of which 640 were upregulated and 1153 were downregulated. Gene Ontology (GO) enrichment analysis revealed that the DEGs were significantly enriched in functional categories related to the cell membrane, cofactors, and carbohydrate energy metabolism. In KEGG metabolic pathway analysis, 278 KEGG pathways were identified, which were enriched mainly in the biosynthesis, carbon metabolism, and amino acid metabolism of secondary metabolites. The results revealed that the enhanced β-glucanase activity in the mutant is likely linked to both the upregulated expression of several genes, including those encoding hemicellulose hydrolases, trehalase, γ-aminobutyrate aminotransferase, and phosphoenolpyruvate carboxykinase, and increased levels of metabolites, such as palmitic acid and linolenate.**

Keywords *Trichoderma reesei*, β-glucanase, Metabolomics, Transcriptomics

β-Glucanase is a collective term for enzymes that can hydrolyze glucan in cereals, including β-(1,3–1,4)-glucanase, endo-, and exo-β-1,3-glucanase, and endo-, and exo-β-1,4-glucanase. During beer brewing, β-glucanase solves the problem of slow wort and beer filtration rates caused by the glucan in barley[1]. The addition of β-glucanase to barley feed can eliminate anti-nutritional factors in the endosperm cell wall, improve nutrient utilization[2], alter material structure, reduce viscosity[3], affect intestinal structure and microbiota, and enhance animal immunity[4]. β-Glucanase is additionally employed in the conversion of biomass to bioethanol and is thus deemed to possess considerable application potential in the realm of bioenergy production[5].

However, industrial production of glucanase faces issues such as low enzyme activity, high cost, and poor thermal stability. Breeding microbial strains with high β-glucanase activity, and good enzyme thermal stability is a research hotspot[6]. Notably, the glucanase gene PsBg16 A from *Paecilomyces* sp. FLH30 was successfully expressed in *Pichia pastoris*, yielding an exceptional enzyme activity of 61 754 U/mL in a 5 L fermenter, which was the highest glucanase activity reported[7]. Furthermore, *Arthrobacter* KQ11 was mutagenized by atmospheric and room temperature plasma (ARTP), resulting in a mutant strain, 4–13, with a β-glucanase activity of 6.27 U/mL, which 1.5 times higher than that of the original strain[8]. Similarly, *Trichoderma reesei* GIMCC 3.498 produced glucanase activity of 37.8 U/mg, representing a high-yield glucanase strain of *T. reesei*[9]. *T. reesei* is safe, non-toxic, enzyme-rich, and its extracellular enzymes can be easily separated[10]. These studies demonstrate that β-glucanase activity can be significantly enhanced through mutation breeding and host expression system optimization. A deeper understanding of the molecular mechanisms underlying strain performance improvement, however, requires the application of emerging omics technologies to elucidate the intrinsic regulatory networks.

The rapid advancement of omics technologies has enabled researchers to elucidate the molecular mechanisms of enzyme production at a systems biology level[11]. Currently, Metabolomics provides a comprehensive overview of metabolic networks by analyzing intracellular metabolites, although sample quenching can be more challenging

[1]Institute of Microbiology, Xinjiang Academy of Agricultural Sciences, Urumqi 830091, China. [2]Xinjiang Laboratory of Special Environmental Microbiology, Urumqi 830091, China. [3]Xinjiang Tiankang Feed Technology Co., Ltd., Wujiaqu 831300, China. ✉email: loukai@tsinghua.org.cn; xiangdonghuo@163.com

than with extracellular metabolites[12]. While other methods provide a general overview, transcriptomics accurately measures the dynamic alterations in gene expression in response to specific conditions, thus reflecting global transcriptional differences induced by mutations[13]. Comparative transcriptome analysis of *T. atroviride*, *T. viride*, and *T. reesei* revealed that multiple β-glucanase and protease genes were upregulated in the transcriptome of *T. atroviride*. *T. viride* upregulated gliotoxin synthesis genes, whereas *T. reesei* expressed many cellulase and hemicellulase synthesis genes before they were physically in contact with alien hyphae[14]. In the presence of *Fusarium oxysporum* f.sp. *momordicae* SG-15 co-culture induction, transcriptome data analysis revealed that *Talaromyces purpureogenus* Q2 upregulated the β-glucanase-related genes *TP1.g228* and *TP2.g877*, speculating that *Talaromyces purpureogenus* Q2 could destroy *F. oxysporum* SG-15 cell wall integrity by producing β-1,3-glucanase and other cell wall-degrading enzymes[15,16]. Under carbon starvation, various β-glucanase genes (An01g04560, An01g03090, An02g13180, and An01g11010) were upregulated in *Aspergillus niger* according to transcriptome analysis[17].

Building upon advances in transcriptomics and metabolomics analytical techniques, modern omics research now achieves multi-dimensional integration[18]. Using proteomic analysis, de Oliveira et al. reported that D-maltose induction caused an increase in microsomal proteins related to translation (e.g., Rpl15) and vesicular transport (e.g., the endosomal-cargo receptor Erv14), promoting fungal utilization of polysaccharide substrates through extracellular digestion catalyzed by secreted enzymes[19]. Zhu reported that the key proteins that degrade lignin model compounds include catechol dioxygenase, glutathione reductase, dextranase, isoamyl alcohol oxidase, glyceraldehyde-3-phosphate dehydrogenase and superoxide dismutase via proteomics and metabolomics analysis of *Aspergillus fumigatus* G-13[20]. These multi-omics strategies provide a systemic perspective for elucidating the mechanisms behind improved enzyme activity in *T. reesei* ARTP mutants. Future studies can integrate data mining to identify key regulatory targets.

In this study, *T. reesei* CICC 2626 was used as the starting strain, and ARTP mutagenesis technology with simple operation, non-polluting environment, and high mutation rate was used. Combined with Congo red-β-glucanase transparent circle screening and enzyme activity rescreening, a genetically stable, high activity β-glucanase strain was obtained. Through metabolomic and transcriptomic analyses, the adaptive changes in the strain to mutations were preliminarily analyzed, which provided the basis for subsequent rational modifications.

Results

ARTP mutant screening

At a treatment time of 120 s, strain CICC 2626 exhibited a lethality rate of 86.96% (Fig. 1). Previous literature has shown that the probability of obtaining forward mutations is higher when the lethality rate is between 85 and 95%[21]. Therefore, a treatment time of 120 s was selected for subsequent experiments.

Based on the ratio of the Congo red hydrolysis transparent circle diameter (H) to the colony diameter (C) (Table 1), 4 mutants were obtained via primary screening and shaking tube rescreening. The enzymatic activity of the mutant strain ARTP-3 was 45.69 U/mL, which was 61.22% higher than that of the original strain.

Transgenerational stability of mutant enzyme activity

The stability of enzyme activity of the original strain and the four mutant strains with higher enzyme activity obtained by rescreening were tested (Table 2). Although the mutant strain ARTP-3 presented the best enzyme activity during rescreening, the enzyme activity was lower than that of the original strain during the passage. The mutant strains ARTP-5 and ARTP-10, despite their augmented enzymatic activity, are prone to instability, which is subsequently compounded by a significant attenuation of enzymatic activity subsequent to 5–7 serial passages, ultimately resulting in a reversion to a level equivalent to that of the original strain. This may be attributed to the accrual of genetic mutations resulting from cellular repair mechanisms triggered by mutagenesis, which manifest as a progressive decline in strain integrity and concomitant loss of desirable traits over successive passages. The enzymatic activity of ARTP-9 was not significantly different ($P > 0.05$) over seven consecutive passages. The β-glucanase activity of ARTP-9 was significantly higher than that of the original *T. reesei* CICC 2626 strain ($P < 0.05$). Therefore, this strain was selected for the subsequent experiments.

Biomass and enzyme activity

After 48 h of culture, the biomass of ARTP-9 reached 3.62 g/L, which was 2.26 times higher than that of the original strain. At 96 h, the biomass reached 10.81 g/L, which was 4.0% higher than that of the original strain ($P < 0.05$). The enzyme activities of the mutant strain ARTP-9 and the original strain CICC 2626 reached the peak at 96 h, and the differences were the greatest, which were 45.12 U/mL and 28.88 U/mL, respectively (Fig. 2). At this point, the mutant strain exhibited an enzyme activity of 4173.91 U/g biomass, whereas the parental strain showed 2834.15 U/g biomass. This represents a 47.27% increase in enzyme activity for the mutant strain compared to the parental strain. Thus, the major effect of the mutation appeared to be enhanced β-glucanase activity. At this stage, mycelia were collected for metabolomic and transcriptomic analyses to analyze the response mechanism of the strain to the mutation.

Metabolomics data quality assessment

The Base Peak Chromatogram current diagram is a spectrum obtained by the continuous scanning of the components separated by chromatography and detected by mass spectrometry, generated by plotting the intensity of the most abundant ion (base peak) at each retention time during LC–MS analysis. It aids in visualizing dominant components in complex samples. In this study, each sample map showed similar trends, with small fluctuations in retention time and peak intensity response position (Fig. 1S). This indicates a stable signal detection, good experimental repeatability, and reliable results.

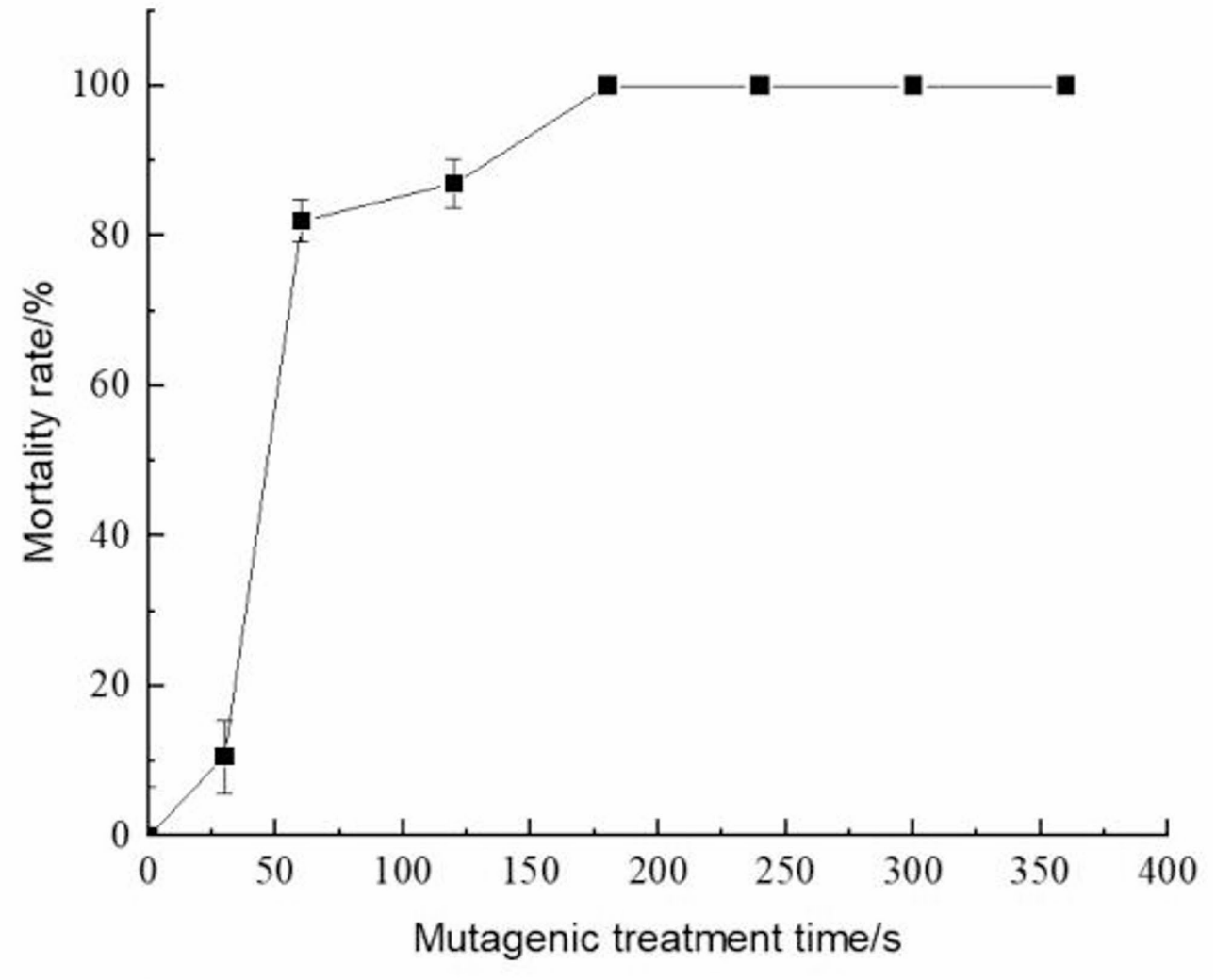

Fig. 1. ARTP-induced Mortality Curve of *T. reesei* CICC 2626.

Strains	Transparent circle diameter (H) /cm	Colony diameter (C)/cm	Hydrolysis ability H/C	β-glucanase activity/U·mL^{-1}	*P* value
CICC 2626	1.60	1.40	1.14	28.34 ± 2.57^{a}	
ARTP-3	1.70	1.40	1.21	45.69 ± 3.92^{b}	0.001
ARTP-5	1.70	1.40	1.21	32.53 ± 0.24^{a}	0.425
ARTP-9	1.90	1.50	1.27	43.75 ± 1.82^{b}	0.001
ARTP-10	1.80	1.40	1.29	40.78 ± 3.76^{b}	0.002

Table 1. Positive mutants of *T. reesei* CICC 2626. Significant differences ($P < 0.05$) are presented as lowercase letters. The data were analyzed by ANOVA, followed by Duncan's multiple range test for multiple comparisons.

Multivariate statistical analysis

Partial Least Squares Discriminant Analysis (PLS-DA) is a multivariate statistical analysis of metabolomic data. It combines a regression equation with dimension reduction, eliminates random errors unrelated to research goals, and efficiently extracts intergroup variation information, surpassing unsupervised analysis methods. The metabolite distribution of the mutant strain at 96 h (M4) was relatively distinct from that of the original strain at 96 h (O4), with model interpretability $R^2 = 0.999$, indicating that the PLS-DA model effectively predicted metabolite differences between the groups (Fig. 3).

Screening of differentially abundant metabolites

A total of 23 differentially abundant metabolites were annotated from the first-level substance list of the quality control samples ($P < 0.05$, variable importance in projection > 1). Compared with those in the original strain

Strains	β-glucanase activity/U·mL^{-1}						
	1st generation	2nd generation	3rd generation	4th generation	5th generation	6th generation	7th generation
CICC 2626	28.83 ± 1.44^{a}	30.33 ± 2.52^{a}	25.61 ± 1.19^{a}	19.46 ± 0.44^{c}	23.82 ± 0.49^{b}	23.7 ± 0.80^{b}	25.2 ± 0.56^{b}
ARTP-3	24.84 ± 3.7^{a}	25.01 ± 2.75^{a}	23.84 ± 1.61^{a}	7.38 ± 1.55^{b}	12.66 ± 0.46^{b}	20.83 ± 0.36^{a}	21.73 ± 0.36^{a}
ARTP-5	29.1 ± 0.06^{c}	34.18 ± 0.54^{b}	30.62 ± 0.65^{bc}	40.01 ± 3.97^{a}	21.05 ± 1.52^{d}	24.11 ± 1.09^{d}	24.36 ± 0.41^{d}
ARTP-9	40.62 ± 1.21^{a}	40.68 ± 0.59^{a}	38.85 ± 0.19^{a}	40.66 ± 0.89^{a}	41.51 ± 2.24^{a}	40.17 ± 0.94^{a}	40.33 ± 0.31^{a}
ARTP-10	34.05 ± 1.55^{b}	38.18 ± 0.85^{a}	38.81 ± 0.99^{a}	41.02 ± 1.02^{a}	27.13 ± 1.37^{c}	28.14 ± 1.15^{c}	25.94 ± 0.42^{c}

Table 2. Transgenerational stability of mutant enzyme activity. Different lowercase letters indicate significant differences ($P < 0.05$) between the mutant strains at different passage times. The data were analyzed by ANOVA, followed by Duncan's multiple range test for multiple comparisons.

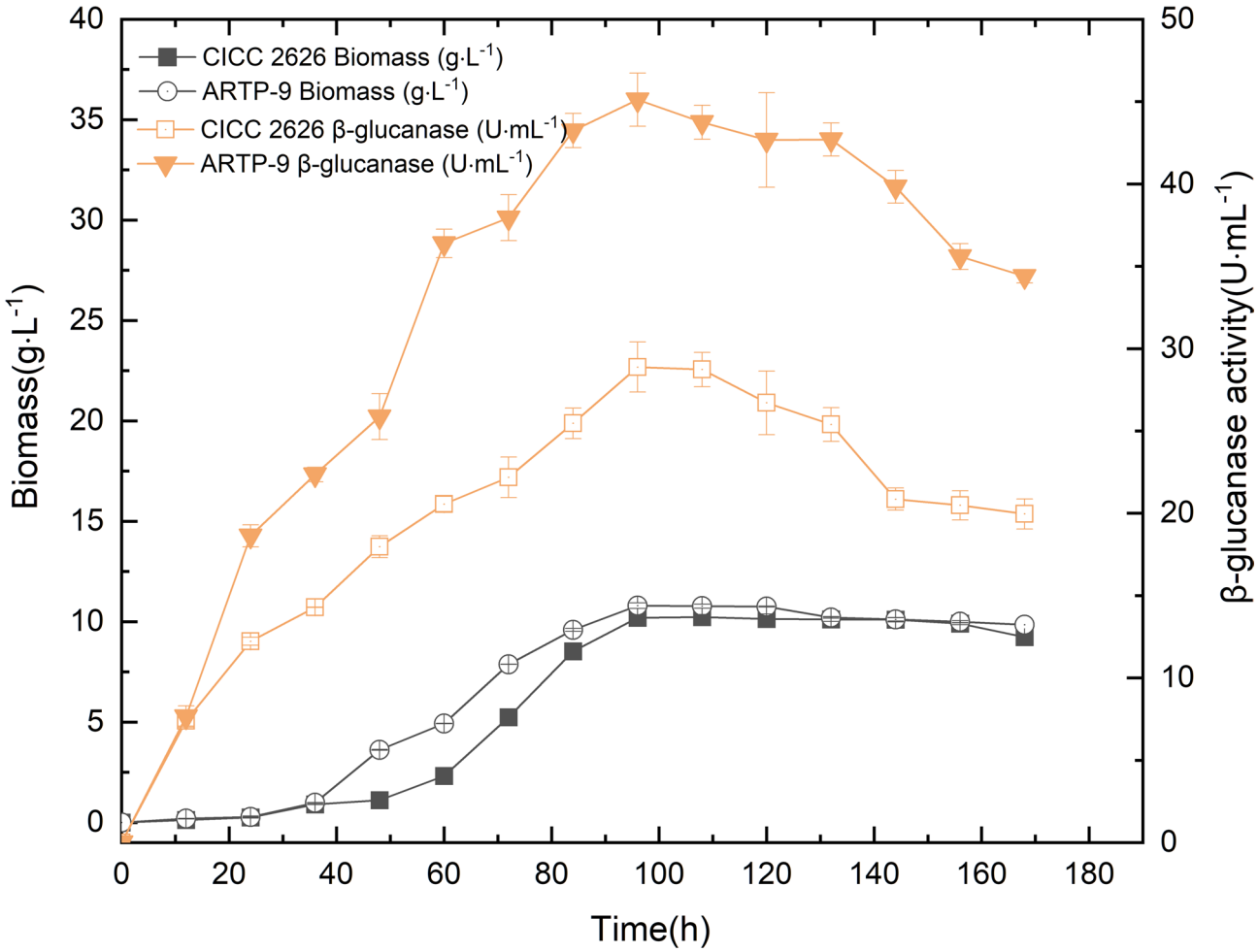

Fig. 2. Monitoring of *T. reesei* CICC 2626 and mutant strain ARTP-9 growth and β-glucanase activity in a 500 mL shake flask under uncontrolled pH conditions.

group, there were 11 significantly upregulated and 12 significantly downregulated metabolites. The expression levels of these metabolites are shown in Table 3. The hierarchical clustering results divided the samples into two categories, M4 and O4, indicating that the 23 differentially abundant metabolites represented the overall differences between the mutant and original strains (Fig. 4).

Transcriptomic data quality assessment

After removing unreliable data from the transcriptomic libraries, 41,616,404 and 41,864,512 data were obtained from the original and mutant strains, respectively. The Q30 exceeded 91%, the mismatch rate was below 0.03%, and there was no significant deviation between bases A, T, G, and C (Table 1S). Therefore, the sequencing data were considered valid for subsequent analyses.

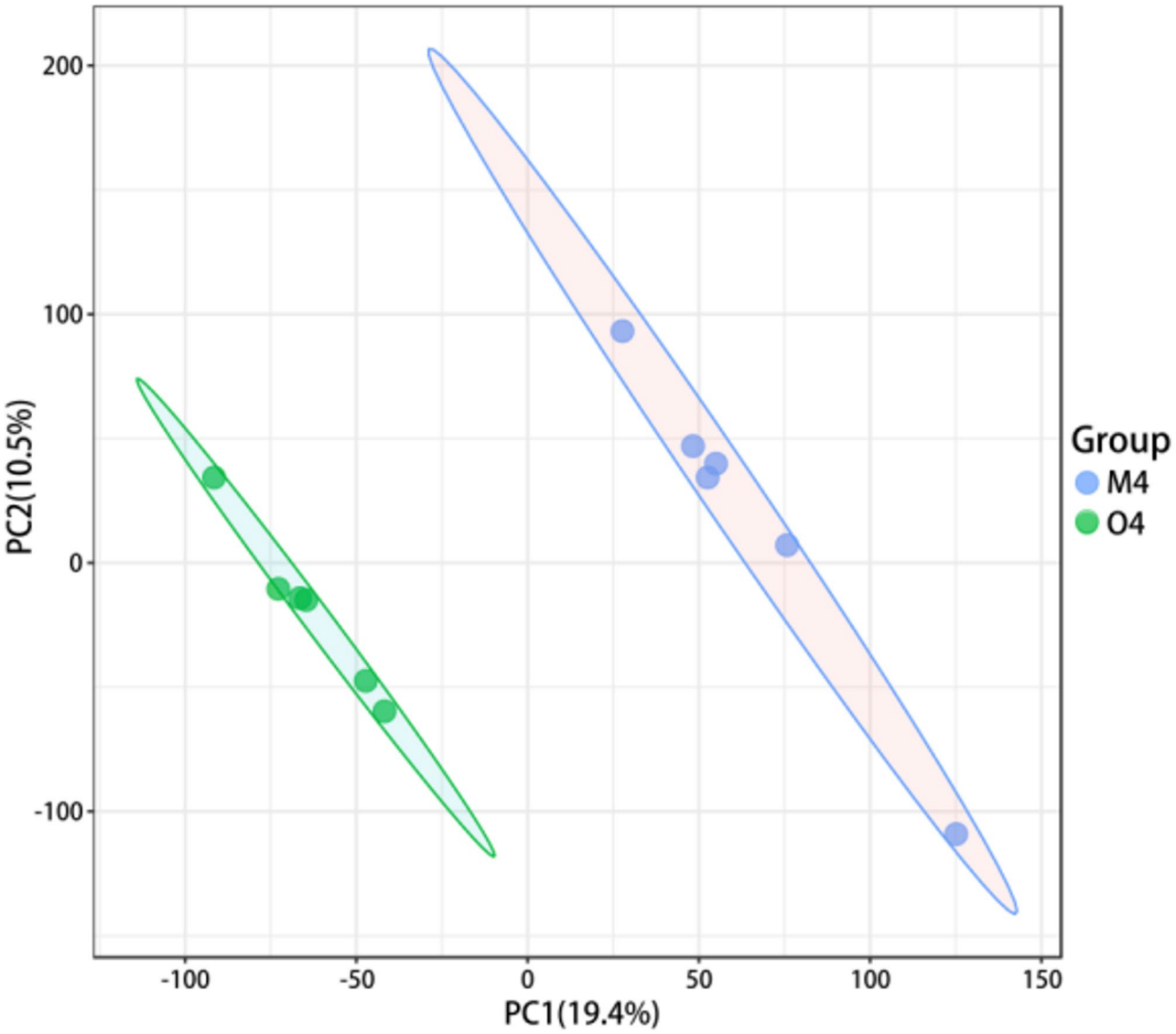

Fig. 3. Partial Least Squares-Discriminant Analysis (PLS-DA) score plot. Under optimal conditions for peak enzyme activity at 28 °C with shaking for 96 h, both *T. reesei* CICC 2626 and the mutant strain ARTP-9 were subjected to PLS-DA. In the score plot, each point represents an individual sample, with green dots representing the O4 (*T. reesei* CICC 2626, n = 6) and blue dots representing the M4 (mutant strain ARTP-9, n = 6). The shaded ellipses in the PLS-DA score plot represent the 95% confidence interval estimated from the score. The x- and y-axes represent the variances associated with components 1 and 2, respectively.

Comparative transcriptomic analysis

To investigate the influence of mutations on gene expression in *T. reesei* CICC 2626, a comparative transcriptomic analysis was performed. The volcanic map of the significant DEGs between the original and mutant strains revealed 640 and 1153 DEGs associated with high and decreased expression of ARTP-9, respectively (Fig. 5A). Cluster analysis of the DEGs in the two groups revealed that the different replicates clustered together under the same treatment, indicating that the gene expression levels of the replicates were highly correlated. The difference between treatments was large, indicating that ARTP caused a significant change in the expression of the mutant ARTP-9 gene (Fig. 5B). KEGG enrichment analysis revealed that the top four pathways most significantly upregulated in the mutant strain ARTP-9 were carbon metabolism (KEGG: ko01200); inositol phosphate metabolism (KEGG: ko00562); propanoate metabolism (KEGG: ko00640); and valine, leucine, and isoleucine degradation (KEGG: ko00280) (Fig. 5C). The top four pathways most significantly regulated in the mutant strain ARTP-9 with decreased expression were biosynthesis of secondary metabolites (KEGG: ko01110), ABC transporters (KEGG: ko02010), glutathione metabolism (KEGG: ko00480), and cysteine and methionine metabolism (KEGG: ko00270) (Fig. 5D). A total of 1370 DEGs were annotated in the GO database, and 278 were annotated in the KEGG database before and after mutation. The GO database contains three main annotation categories: molecular function, cellular component, and biological process. A total of 257 secondary entries and

Metabolite	Molecular formula	log2FC	*P* value	VIP
Upregulated expression				
beta-Alanyl-L-lysine	$C_9H_{19}N_3O_3$	6.17	0.04	1.42
2-Heptanone	$C_7H_{14}O$	2.64	0.02	2.10
Linatine	$C_{10}H_{17}N_3O_5$	2.39	0.00	2.34
Gentamicin C1a	$C_{19}H_{39}N_5O_7$	1.76	0.00	1.80
2,4-Dihydroxypteridine	$C_6H_4N_4O_2$	1.53	0.04	1.65
3-Methylthiopropionic acid	$C_4H_8O_2S$	1.11	0.03	1.79
Terephthalate	$C_8H_6O_4$	0.90	0.03	1.66
Taurine	$C_2H_7NO_3S$	0.88	0.04	1.40
*N*7-Methylguanosine	$C_{11}H_{16}N_5O_5$	0.84	0.04	1.38
Pyridoxal phosphate	$C_8H_{10}NO_6P$	0.83	0.04	1.11
Palmitoleic acid	$C_{16}H_{30}O_2$	0.76	0.00	2.28
Downregulated expression				
Beta-Carboline	$C_{11}H_8N_2$	− 1.86	0.00	1.95
N-Acetyl-beta-glucosaminylamine	$C_8H_{16}N_2O_5$	− 1.60	0.04	1.69
L-Histidinol	$C_6H_{11}N_3O$	− 1.45	0.02	1.57
CMP	$C_9H_{14}N_3O_8P$	− 1.17	0.00	2.28
Spermine	$C_{10}H_{26}N_4$	− 0.88	0.04	1.58
Niacinamide	$C_6H_6N_2O$	− 0.86	0.02	1.73
Glutathione	$C_{10}H_{17}N_3O_6S$	− 0.86	0.02	1.51
(R)-Pantolactone	$C_6H_{10}O_3$	− 0.83	0.00	2.45
Stearidonic acid	$C_{18}H_{28}O_2$	− 0.69	0.04	1.59
S-Adenosylhomocysteine	$C_{14}H_{20}N_6O_5S$	− 0.65	0.01	1.58
Nonadecanoic acid	$C_{19}H_{38}O_2$	− 0.63	0.00	1.18
Isophorone	$C_9H_{14}O$	− 0.59	0.03	1.81

Table 3. Differentially abundant metabolite information. Metabolites exhibiting upregulated expression were observed in the mutant strain ARTP-9 (M4) compared to the *T. reesei* CICC 2626 (O4). Conversely, other metabolites showed downregulated expression in M4 relative to O4. A log2 fold change (log2FC) ≥ 1 was used to define upregulated metabolites, while a log2FC ≤ − 1 indicated downregulated metabolites. Variable importance in projection (VIP) refers to the relative influence of each metabolite in the group; metabolites with higher VIP values are more influential.

518 genes were annotated to the biological process category, among which DNA replication (GO: 0,006,260), DNA metabolic processes (GO: 0,006,259), and carbohydrate metabolic processes (GO: 0,005,975) were significantly different ($P < 0.05$) (Fig. 6A). A total of 179 genes from 53 secondary entries were annotated to the cell component category (Fig. 6B). There were significant differences in the composition of the membrane (GO: 0,016,021), inherent composition of the membrane (GO: 0,031,224), and membrane region (GO: 0,044,425) ($P < 0.05$). A total of 673 genes from 184 s-level entries were annotated to the molecular function category, of which iron ion binding (GO: 0,005,506), co-factor binding (GO: 0,048,037), and hydrolase activity, acting on acid anhydrides (GO: 0,016,817), were significantly different ($P < 0.05$) (Fig. 6C). The metabolism, material transport, and signal transduction of the mutant strain ARTP-9 were significantly different from those of the original strain *T. reesei* CICC 2626.

DEGs related to β-glucanase

KEGG metabolic pathway annotation of the DEGs revealed 85 metabolic pathways. To identify upregulated differential genes related to β-glucanase, and explore the reasons for increased enzyme activity caused by mutations, DEGs were screened using log2 fold change > 1 and $P < 0.05$. Five significantly upregulated DEGs were identified (Table 4). These DEGs were mainly related to biological regulation, cellular processes, energy metabolism, and catalytic activity. These genes included those encoding β-1,3-glucanase (GH64) and α,α-trehalase (GH37), which are related to hydrolases in starch and sucrose metabolic pathways, as well as those encoding γ-aminobutyric acid transferase and dihydrolipoic acid transacetylase, which are involved in amino acid metabolism and propionic acid metabolic pathways. In addition, the genes encoding phosphoenolpyruvate carboxykinase are involved in glycolysis. These findings indicate that the increased expression of genes related to hydrolase synthesis and energy metabolism may be the reason for the increased activity of β-glucanase in the *T. reesei* mutant strain ARTP-9.

Association analysis

KEGG analysis of the DEGs revealed that palmitic acid promoted the upregulation of γ-aminobutyric acid transferase in the amino acid metabolic pathway, thereby enabling cross-linking between proteins. Pyridoxal phosphate, a coenzyme, stabilizes various enzymes. Taurine increases the ER volume, and promotes protein

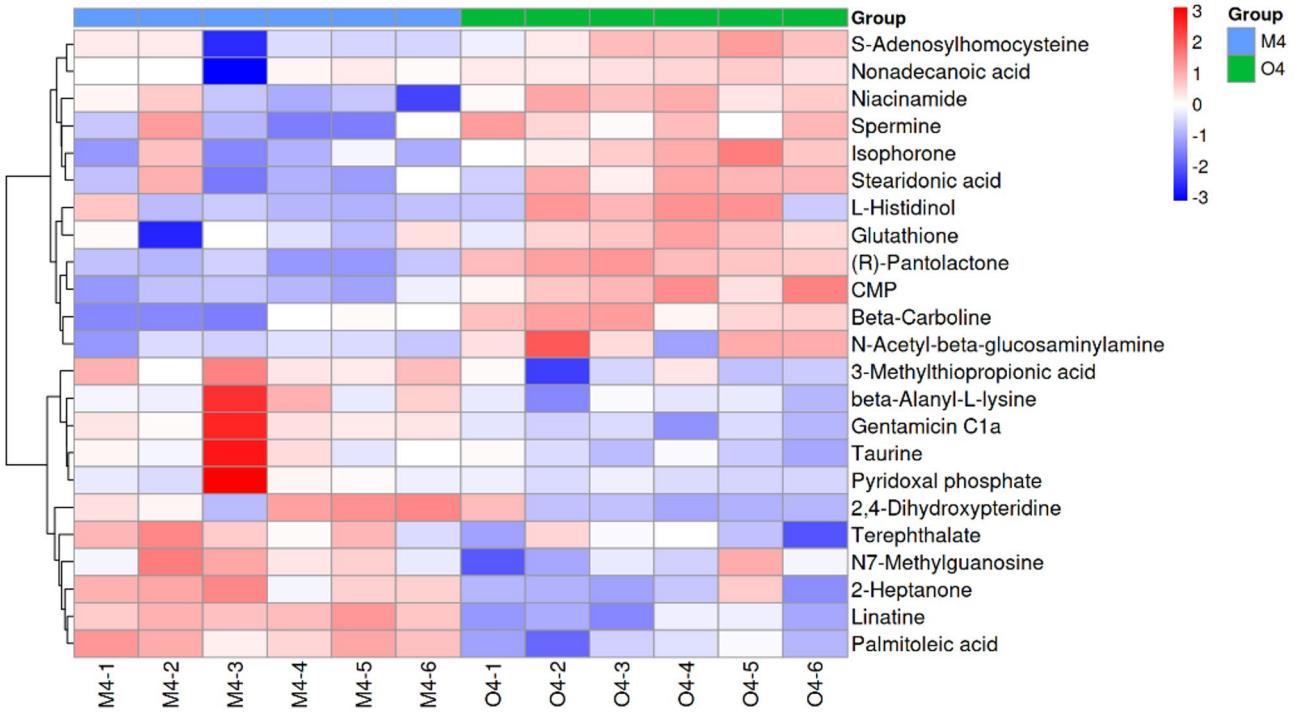

Fig. 4. Heatmap analysis of differential metabolites in O4(*T. reesei* CICC 2626) and M4 (mutant strain ARTP-9) under optimal conditions for peak enzyme activity at 28 °C with shaking incubation for 96 h. Heatmap analysis of differential metabolites obtained by Student's t-test model analysis (false discovery rate, $P < 0.05$) of mycelia (n = 10). The red and blue colors in the plot indicate high and low intensities, respectively, and the values ranges from −3 to + 3.

synthesis and secretion. Taurine and linolenic acid contents increased during oxidative stress, with upregulated expression of dihydrolipoic acid transacetylase in the nucleic acid synthesis pathway, indicating accelerated nucleic acid synthesis in the mutant. The upregulated expression of phosphoenolpyruvate carboxylase during glycolysis indicates accelerated energy metabolism in the mutant. Trehalase can alter solution hypertonicity and promote the secretion of the extracellular hydrolase β-1,3 glucanase (Fig. 7).

Discussion

In this study, a mutant strain, ARTP-9, with β-glucanase activity of 45.12 U/mL was selected from *T. reesei* CICC 2626 mutagenesis by ARTP, which was 56.23% higher than that of the original strain and was genetically stable. The metabolic responses observed in microbes induced by ARTP have been documented[22]. LC-MS non-targeted metabolomics analysis revealed that, compared with the original strain group, β-alanyl-L-lysine was increased in the 96 h mutant group in this study. β-Alanyl-L-lysine, a dipeptide of β-alanine and L-lysine, has also been shown to be significantly upregulated during the spore formation of *Bacillus subtilis* 168, as demonstrated by capillary electrophoresis mass spectrometry[23]. It was hypothesized that carnosine-related dipeptides function as potent endogenous antioxidants[24]. Linolenic acid content was increased in the mutant. Acetyl-CoA directly participates in lipid metabolism, producing linolenic acid, an amino acid derivative of pyrrolidine dicarboxylic acid, carbohydrazide, and D-proline. When cultivated on glucose, strains of the genera *Zygorhynchus*, *Mortierella*, *Rhizopus*, *Mucor*, and *Cunninghamella* produce significant quantities of γ-linolenic acid[25]. Linolenic acid and antioxidants, such as α-lipoic acid and 3,3-methoxyphenylhydrazine, have protective effects against DNA damage and apoptosis in insulin-secreting cell lines and primary human fibroblasts[26]. In this study, linolenic acid expression was upregulated in the mutant strain, linolenic acid content was significantly positively correlated with β-glucanase activity, with a protective effect against oxidative stress, which may be involved in biological processes, such as DNA damage repair and growth inhibition. 7-Methylguanosine was increased in the mutant. 7-Methylguanosine is a post-transcriptional modification of eukaryotes that exists in the cap structure at the 5' end of the mature mRNA. It is also a product of purine metabolism, and is associated with oxidative stress [27]. Taurine is a 2-amino derivative of ethanesulfonic acid. It is a naturally occurring amino acid that is derived from the metabolism of methionine and cysteine. It has many biological effects, such as bile salt binding, antioxidant effects, osmotic pressure regulation, membrane stability regulation, and calcium signal transduction[28]. Taurine is regarded as a cytoprotective molecule owing to its ability to sustain a normal electron transport chain, maintain glutathione stores, upregulate antioxidant responses, increase membrane stability, eliminate inflammation, and prevent calcium accumulation. In parallel, the synergistic effects of taurine and other potential therapeutic modalities for multiple disorders have been highlighted[29]. In this study, the content of taurine in the mutant increased, which induced an increase in endoplasmic reticulum volume and increased

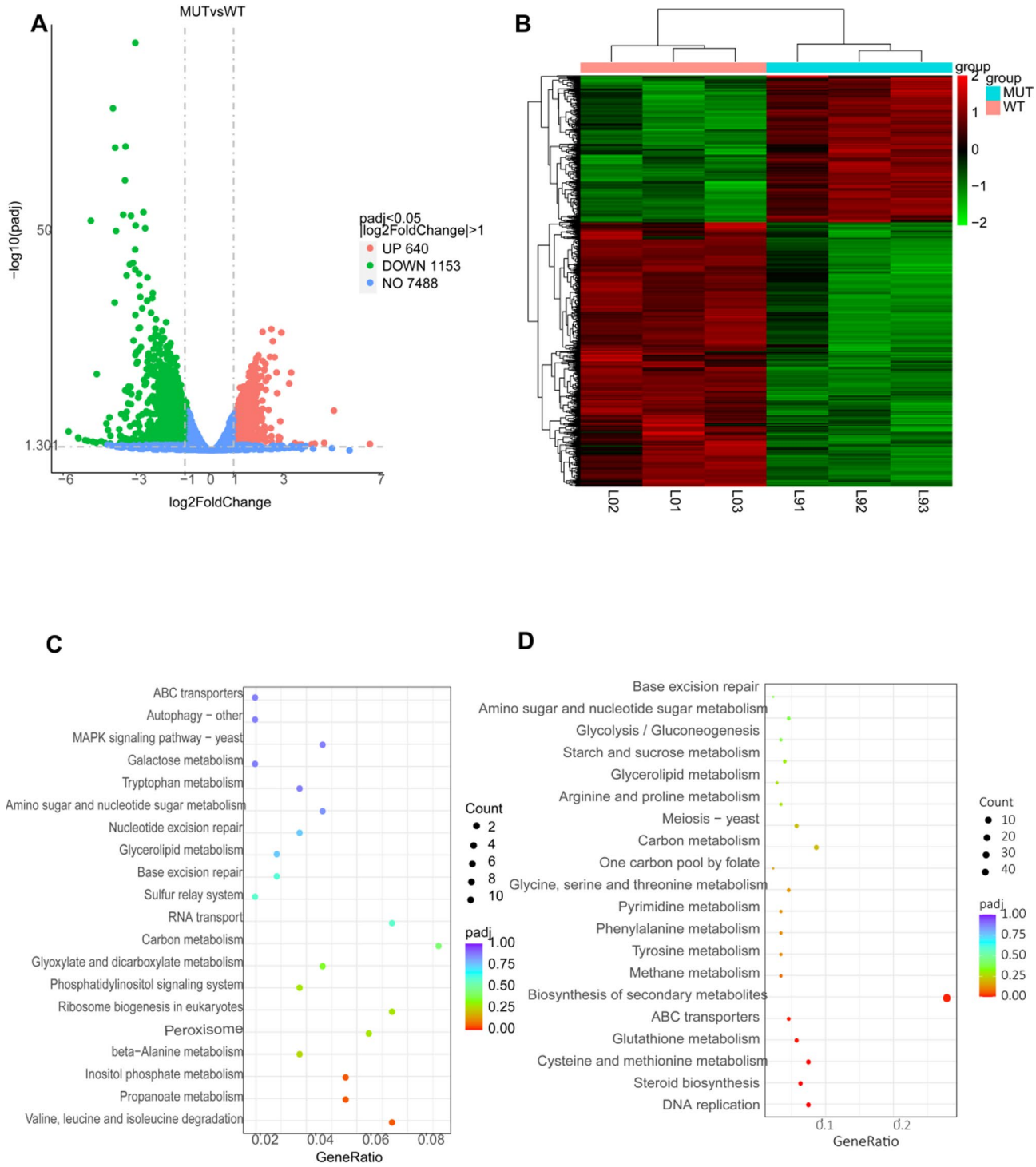

Fig. 5. Transcriptomic comparison of the mutant strain ARTP-9 and the original strain *T. reesei* CICC 2626. (**A**) Volcanic map of differentially expressed genes in comparable groups. (**B**) Cluster heatmap of differential gene expression levels. (**C**) KEGG enrichment analysis of upregulated metabolic pathways ($P < 0.05$). (**D**) KEGG enrichment analysis of downregulated metabolic pathways ($P < 0.05$). The data were analyzed by ANOVA, t-test, and Duncan's multiple range test for multiple comparisons.

protein production while exerting the above functions. In this study, the expression of pyridoxal phosphate was upregulated. Pyridoxal phosphate (PLP), the active form of vitamin B6, acts as an electrophilic catalyst to stabilize a variety of enzymatic reactions as a coenzyme[30]. Therefore, ARTP may improve β-glucosidase secretion in the mutant strain by altering biological processes, such as protein synthesis, oxidative stress protection, and enzymatic reaction regulation.

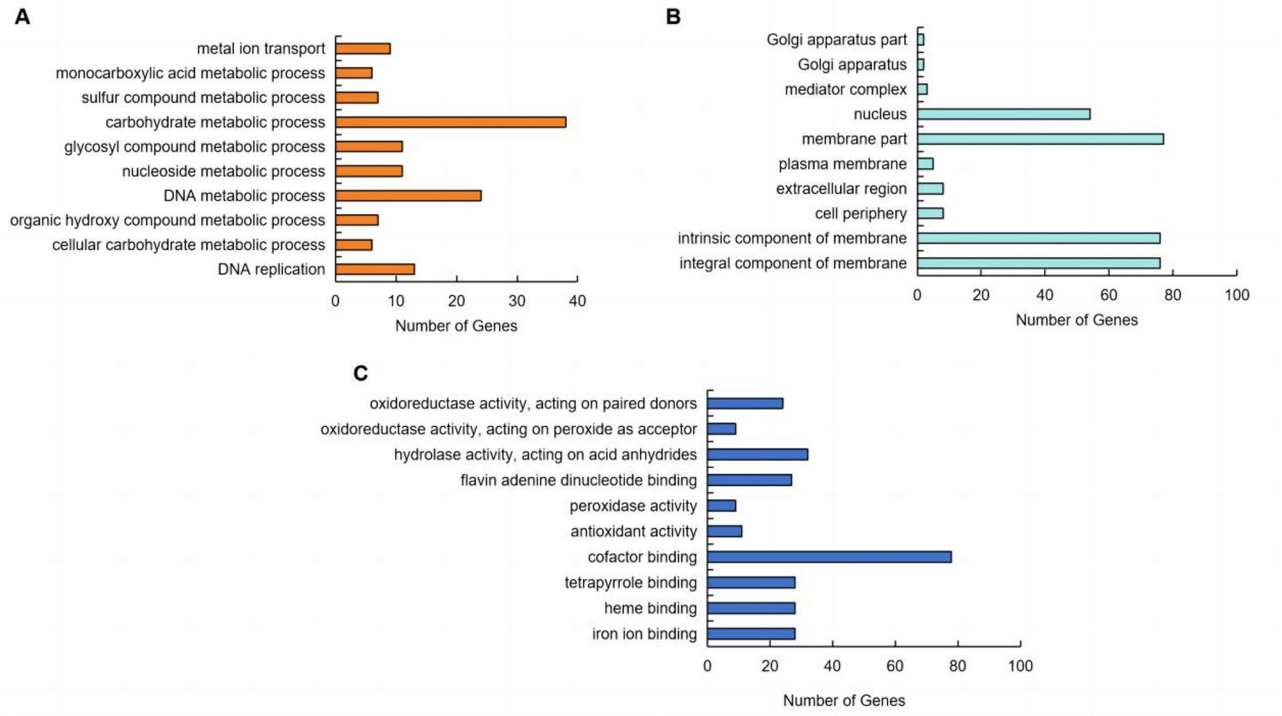

Fig. 6. GO enrichment function classification map of the DEGs ($P < 0.05$). (**A**) Terms related to biological processes are colored in orange. (**B**) Terms related to cellular components are colored in sky blue. (**C**) Terms related to the molecular functions are colored in blue. Classification of the complete transcriptomes by type after Blast2GO Enrichment Analysis. Pinpoint the biological categories with the greatest overrepresentation of DEGs. The data were analyzed by ANOVA, t-test, and Duncan's multiple range test for multiple comparisons.

Gene No.	Gene ID	log2 fold change	GO function	KEGG pathway
18,483,689	TRIREDRAFT_123639	4.12	β-1,3-glucanase(GH64)	Starch and glucose metabolism
18,483,595	TRIREDRAFT_123226	2.87	α, α-trehalase(GH37)	Starch and glucose metabolism
18,483,143	TRIREDRAFT_121405	2.23	γ-aminobutyric acid transferase	Amino acid metabolism, Propionic acid metabolism
18,482,885	TRIREDRAFT_120473	2.10	dihydrolipoic acid transacetylase	Amino acid metabolism, Propionic acid metabolism
18,483,813	TRIREDRAFT_124115	1.82	phosphoenolpyruvate carboxylase	Glycolysis metabolism

Table 4. Functions and metabolic pathways of the significantly upregulated genes in the mutant strain ARTP-9 compared to those in *T. reesei* CICC 2626. Log2 fold change values represent the log2-transformed ratio of gene expression between the two samples. An increased log2 fold change value indicates a greater degree of upregulation of a specific gene in the mutant ARTP-9 strain versus the *T. reesei* CICC 2626 strain.

The synthesis and secretion of β-glucosidase are regulated by various pathways. In this study, transcriptomic sequencing of the original strain CICC 2626 and mutant strain ARTP-9. GO function and KEGG pathway enrichment analyses revealed that the mutation led to changes in DNA replication, amino acid metabolism, and carbohydrate metabolism in *T. reesei*. The differentially expressed genes were involved in starch and sucrose, propionic acid, amino acids, glycolysis, and other metabolic pathways. Among these genes, β-glucanase genes are mainly involved in the starch and sucrose metabolic pathways (tre00500). The significantly upregulated genes in this pathway included β-1,3-glucanase of the glycoside hydrolase family (GH) 64 and α, α-trehalase of GH37. A previous study reported that genes related to N-glycosylation and starch and sucrose metabolic pathways were significantly upregulated in mutants during the study of a high-yield *Trichoderma longibrachiatum* strain induced by heavy ion beam mutagenesis and its cellulase production mechanism. The key candidate genes affecting cellulase secretion were Sec61, PDI, and VIP36[31]. β-glucanase is an inducible enzyme. Under glucan substrate conditions, the expression of β-glucanase-related genes in the mutant strain ARTP-9 was upregulated, glucan hydrolysis was enhanced, cell growth and metabolism were promoted, and enzyme activity was increased. Trehalose, a cellular stress metabolite, is related to the hypertonic nature of shake flask cultivation solutions[32]. The expression of γ-aminobutyric acid transaminase (EC: 2.6.1.22) was also upregulated. γ-Aminobutyric acid transaminase is located at the core of the protein interaction network, where it is involved in enhanced amino acid transport activities, and is closely associated with protein synthesis and secretion. Dihydrolipoic acyltransferase

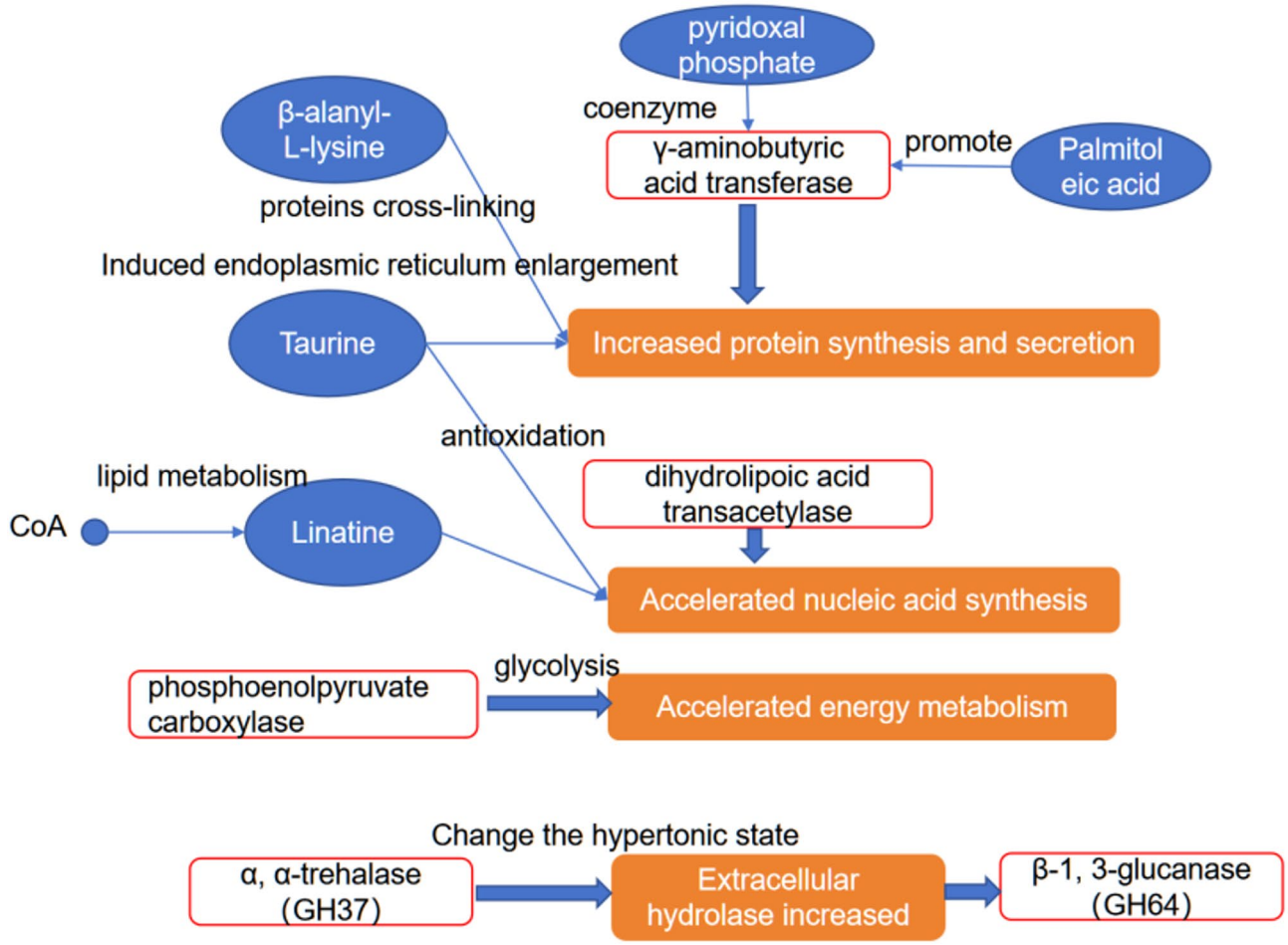

Fig. 7. Association network diagram of DEGs and metabolites between *T. reesei* CICC 2626 and mutant strain ARTP-9. Red rectangles represent enzyme types identified by comparative transcriptomic screening; Blue ovals represent differential metabolites; Orange rectangles represent the biological processes involved.

catalyzes the oxidative decarboxylation of pyruvate to acetyl-CoA by acetyl-phosphogluconate dehydrogenase, thereby increasing nucleic acid synthesis[33]. In this study, the expression of dihydrolipoic acyltransacetylase (EC: 2.3.1.168) gene in the mutant strain ARTP-9 was upregulated, and it was speculated that its nucleic acid synthesis rate accelerated accordingly. The expression of phosphoenolpyruvate carboxykinase (EC: 4.1.1.49) was upregulated during glycolysis, indicating that the metabolic activity of ARTP-9 was enhanced after mutation, and that a large amount of ATP was consumed. Phosphoenolpyruvate carboxykinase catalyzes oxaloacetic acid and ATP to produce phosphoenolpyruvate, ADP, and CO_2.

Multi-omics integration analysis revealed that ARTP mutagenesis upregulated the expression of multiple metabolites and genes related to lipid synthesis, and promoted N-glycosylation and amino acid metabolism. For instance, with increasing palmitic acid levels, differential genes related to arginase, amidase, γ-glutamyltransferase, GAF domain protein, acetate kinase, and acetaldehyde dehydrogenase in the amino acid metabolic pathway were upregulated. Therefore, ARTP mutagenesis may lead to the upregulation of genes encoding extracellular hydrolases, protein synthesis, and Golgi vesicle transport in *T. reesei*, thereby increasing protein synthesis and secretion. These factors are speculated to be responsible for the increase in β-glucanase activity.

Materials and methods

Mortality rate

A 10 µL aliquot of spore suspension was spread on a sterile metal slide. A plasma treatment was conducted using 99.99% high-purity helium as the working gas at a flow rate of 10 SLM, a power of 100 W, and a working distance of 2 mm (i.e., the distance between the slide and the gas outlet). Treatment durations were set at 0, 30, 60, 120, 180, 240, 300, and 360 s. Immediately after each treatment, the slide was promptly transferred into a 1.5 mL microcentrifuge tube containing 990 µL of sterile water. After thorough mixing, the suspension was serially diluted and plated onto PDA agar. Colony-forming units (CFUs) were enumerated for each treatment duration to generate a lethality curve. The calculation of the lethality rate is presented in Eq. 1:

$$\text{Mortality rate } (\%) = (\text{A} - \text{B})\,/\text{A} \times 100 \quad (1)$$

In the equation: *A*: represents the colony count from the plate inoculated with the spore suspension at a treatment time of 0 s (i.e., the initial colony count). *B*: represents the colony count from the plate inoculated with the spore suspension at various treatment times.

Determination of β-glucanase activity

This method involved minor modifications to NY/T 911–2020[34].

β-Glucanase activity: At 50 °C and pH 5.5, the amount of enzyme required to hydrolyze 10 mg/mL β-glucan to produce 1 μmol of glucose per minute was defined as one unit of enzyme activity.

Standard curve: A standard series of glucose solutions with concentrations of 0 mg/mL, 0.1 mg/mL, 0.2 mg/mL, 0.3 mg/mL, 0.4 mg/mL, 0.5 mg/mL, 0.6 mg/mL, 0.7 mg/mL, and 0.8 mg/mL were prepared with acetic acid-sodium acetate buffer.

Two milliliters of the standard series solution were used, and sterile water was used as a blank control. The mixture was placed in a 25 mL test tube with a stopper, and 2 mL of sodium acetate buffer (pH 5.5) and 5 mL of DNS solution were added. After mixing, the mixture was placed in a boiling water bath and boiled for 10 min. After cooling to room temperature, the mixture was diluted to 25 mL. After shaking, 200 μL of the solution was transferred to a microplate reader for the determination of absorbance. The wavelength was set at 540 nm. The absorbance was plotted on the x-axis, and the glucose concentration was plotted on the y-axis to draw a standard curve.

Determination of β-glucanase activity: β-glucan (China and Yuanye Biotechnology Co., Ltd., Shanghai, China. ≥ 95%) solution (150 μL) was pipetted into a 1.5 mL centrifuge tube and incubated in a 50 °C metal bath for 10 min, after which 150 μL of the sample supernatant solution was added. After mixing, the mixture was placed in a 50 °C metal bath for 10 min, and 300 μL DNS solution was added to terminate the enzymatic hydrolysis reaction. After shaking and mixing, the mixture was placed in a boiling water bath for 5 min. After cooling to room temperature, 900 μL distilled water was added. After mixing, 200 μL was transferred to a microplate reader to determine absorbance at 540 nm. The supernatant of the boiled inactivated sample was used as a blank control, and the remaining steps were the same as described above. β-Glucanase activity (X) was calculated via Eq. 2:

$$X = ((C - C0) \times 100 \times N) / (M \times t \times 180.2) \times 1000 \quad (2)$$

where C. The glucose concentrations in the reaction solutions of the samples were tested, mg/mL; C0. Glucose concentration in the blank group, mg/mL; N. The dilution factor of the sample after reaching a constant volume; m. Sample mass, the liquid is in mL, the solid-state is g, and t. enzyme reaction time, min; 100. Constant sample volume, mL; 180.2. Molar mass of glucose, g/mol; 1000. conversion factor, 1 mol = 1000 mmol.

Culture condition

The plate culture conditions for the original *T. reesei* CICC 2626 strain and all mutant strains in this study were maintained at a constant temperature of 28 °C for 96 h, using the medium described below. Similarly, the shake flask cultures were conducted at 28 °C for 96 h with agitation at 180 rpm, utilizing the same specified medium.

Medium

The primary screening medium consisted of 5.0 g/L β-glucan, 3.5 g/L $(NH_4)_2SO_4$, 1.0 g/L K_2HPO_4, 0.5 g/L KCl, 0.5 g/L $MgSO_4$·7H2O, 15 g/L agar. The rescreening medium consisted of 5.0 g/L β-glucan, 3.5 g/L $(NH_4)_2SO_4$, 1.0 g/L K_2HPO_4, 0.5 g/L KCl, 0.5 g/L $MgSO_4$·$7H_2O$. The seed medium consisted of 20.0 g/L glucose, 20.0 g/L peptone, 10.0 g/L yeast extract. The enzyme production medium consisted of 5.0 g/L β-glucan, 4.0 g/L $(NH_4)_2SO_4$, 1.0 g/L K_2HPO_4, 0.5 g/L KCl, 0.4 g/L $MgSO_4$, 0.015 g/L $FeSO_4$, 2.0 g/L Tween 80, 4.0 g/L $CaCl_2$. The reagents were provided by Dingfeng Biotechnology Co., Ltd., Xinjiang, China, and Yuanye Biotechnology Co., Ltd., Shanghai, China.

ARTP mutagenesis

Ten microliters of germinated spores of *T. reesei* CICC 2626 was evenly spread on sterile metal slides. The working gas was 99.999% high-purity helium. The gas flow rate was set to 10 SLM (standard liter per minute), the power was 100 W, the working distance (i.e., the distance between the slide and airflow port) was 2 mm, and the processing time was 120 s. After treatment, the slides were transferred to 990 μL sterile water. After mixing, the mixture was diluted and spread onto PDA plates. Strains with rapid growth and large colonies were selected for further analyses.

Primary screening: The strains were inoculated on primary screening media, cultured at 28 °C for 3 d, and stained with Congo red, and strains with a large ratio of transparent circles to colonies were selected.

Rescreening: The strains obtained from preliminary screening were inoculated on slant media. The spore concentration was adjusted to 10^6 CFU/mL, and a 2% spore mixture was inoculated into the seed medium, which was subsequently cultured at 28 °C and 180 rpm for 30 h. The enzyme production medium was inoculated with 2% seeds, and incubated at 28 °C and 180 rpm for 96 h. Strains with high enzyme activity were selected for subsequent experiments.

Transgenerational stability of mutant enzyme activity

Re-screened, high-activity β-glucanase mutants were passaged seven times. Enzyme activity was monitored to evaluate the stability of the enhanced phenotype. This study investigated whether adaptive changes induced by mutagenesis are stably maintained across generations, and whether reversion during subculturing limits the isolation of stable mutants.

Dynamic curve of β-glucanase for shake flask cultivation

T. reesei CICC 2626 and the mutant strain ARTP-9 were cultured as rescreening procedures, and the enzyme activity of the two strains were determined within 168 h. Biomass was measured every 12 h. A dynamic curve was constructed.

Metabolome analysis

After 96 h of cultivation, *T. reesei* CICC 2626 and ARTP-9 were harvested by centrifugation (4000 × g, 4 °C, 5 min). The cells were separated from the supernatant, washed 3–5 times with ice-cold PBS, and immediately quenched in liquid nitrogen to stabilize intracellular metabolites. The metabolome of *T. reesei* CICC 2626 was O4, and that of ARTP-9 was M4. The liquid chromatography tandem mass spectrometry (LC–MS) metabolomic detection was performed by Panomik Biomedical Technology Co., Ltd.,Suzhou, China.

Liquid chromatography

LC analysis was performed via a Vanquish UHPLC System (Thermo Fisher Scientific, USA). Chromatography was performed using an ACQUITY UPLC® HSS T3 column (150 × 2.1 mm, 1.8 μm) (Waters, Milford, MA, USA). The column was maintained at 40 °C. The flow rate and injection volume were set to 0.25 mL/min and 2 μL, respectively. For LC-ESI (+)-MS analysis, the mobile phase consisted of (B2) 0.1% formic acid in acetonitrile (v/v), and (A2) 0.1% formic acid in water (v/v). The gradient elution procedure for the positive and negative ion modes was performed according to the literature[35].

Mass spectrometry

The mass spectrometric detection of metabolites was performed via an Orbitrap Exploris 120 (Thermo Fisher Scientific, USA) with an ESI ion source. Simultaneous MS1 and MS/MS (Full MS-ddMS2 mode, data-dependent MS/MS) acquisitions were performed. The parameters were as follows: sheath gas pressure, 30 arb; aux gas flow, 10 arb; spray voltage, 3.50 kV and −2.50 kV for ESI(+) and ESI(−), respectively; capillary temperature, 325 °C; MS1 range, 100–1000 m/z; MS1 resolving power, 60,000 FWHM; MS/MS resolving power, 15,000 FWHM; normalized collision energy, 30%.

RNA sequencing

Total RNA extraction and determination

The sample number of the *T. reesei* CICC 2626 transcriptome was L0, and that of the ARTP-9 transcriptome was L9. In this study, total RNA was extracted via the TRIzol method, and the RNA samples were strictly controlled via an Agilent 2100 bioanalyzer. Qualified samples were stored at −80 °C for subsequent cDNA library construction.

cDNA library construction

The NEBNext® UltraTM RNA Library Prep Kit for Illumina® was used for library construction. After library construction was completed, the Qubit2.0 Fluorometer was used for preliminary quantification. To ensure the quality of the library, qRT-PCR was used to accurately quantify the effective concentration of the library, such that the effective concentration of the library was higher than 2 nmol. Illumina NovaSeq 6000 high-throughput sequencing was performed.

Identification of differentially expressed genes (DEGs)

The HISAT2 software was used to compare clean reads with the reference genome of *T. reesei* (*T. reesei* QM6a) to obtain the location information of the reference genome. StringTie software was used to assemble clean reads from scratch to obtain DEGs, and the FPKM value reflected the expression abundance of the corresponding DEGs. In this experiment, three biological replicates were set up, DESeq2 software was used to standardize DESeq, and |log2 fold change) |≥ 1 and P value ≤ 0.05, were used as screening standards to obtain DEGs. GO functional annotation and KEGG pathway enrichment analyses of the DEGs were performed via ClusterProfiler.

Association analysis of metabolomics and transcriptomics

The MetaboAnalyst software package was used to enrich the functional pathways of the differentially abundant metabolites. The KEGG Mapper visualization tool was used to analyze the differentially abundant metabolites[36–38]. Pearson correlation analysis was used to calculate the correlation coefficients between the differentially abundant metabolites and DEGs. Association analysis was performed on the genes and metabolites involved in the same metabolic pathway, and a metabolic association network map was constructed.

Statistical analyses

All experiments were performed in triplicate, and the results are expressed as the mean ± standard deviation. The data were analyzed by ANOVA, t-test, and Duncan's multiple range test for multiple comparisons using SPSS 25.0, with the significance level at $P < 0.05$, while charts were generated with Origin 2021.

Conclusion

In this study, four *T. reesei* mutants exhibiting significantly enhanced β-glucanase activity were successfully isolated using ARTP mutagenesis. Among these, the ARTP-9 mutant demonstrated the highest activity at 45.12 U/mL, representing a 56.23% increase compared with the parental strain, and also exhibited notable stability. Integrated multi-omics analyses were conducted to elucidate the molecular mechanisms underlying the elevated β-glucanase production in ARTP-9. The findings reveal that key regulatory pathways involve metabolic reprogramming to promote enzyme synthesis and secretion, primarily through enhanced protein synthesis and increased cofactor availability, as well as the maintenance of antioxidant capacity and metabolic

homeostasis. For instance, the accumulation of linolenic acid and 7-methylguanosine mitigated oxidative stress, thereby supporting sustained strain growth and enzyme synthesis under high metabolic load. Additionally, several critical genes within the starch and sucrose metabolism pathway, which are directly related to enhanced enzyme activity (e.g., β-1,3-glucanase and α,α-trehalase), were significantly upregulated in the mutant strain. Collectively, the ARTP-9 mutant and its associated multi-omics analyses provide a robust theoretical framework for the molecular breeding of *T. reesei* and establish a technical foundation for the efficient production of industrial enzyme preparations. Future research should focus on validating the direct contributions of taurine and linolenic acid synthesis genes to enzyme activity through overexpression studies, as well as assessing the performance stability of the mutant strain under industrial fermentation conditions.

Data availability

The RNA sequence data were deposited in the National Center for Biotechnology Information (NCBI) Sequence Read Archive (SRA) under the study accession number PRJNA1160021 (https://www.ncbi.nlm.nih.gov/bioproject/?term=PRJNA1160021). All data generated or analyzed in this work are included in this published article. Any other data used and/or analyzed during the current study is available from the corresponding author on reasonable request.

Received: 4 September 2024; Accepted: 18 June 2025
Published online: 12 July 2025

References

1. Kupetz, M. et al. Critical review of the methods of β-glucan analysis and its significance in the beer filtration process. *Eur. Food Res. Technol.* **241**, 725–736 (2015).
2. De Arcangelis, E. et al. Structure analysis of β-glucan in barley and effects of wheat β-glucanase. *J. Cereal Sci.* **85**, 175–181 (2019).
3. Heidary Vinche, M. et al. Investigation of the effects of fermented wheat bran extract containing beta-glucanase on beta-glucan of cereals used in animal feed. *Cereal Chem.* **98**, 651–659 (2021).
4. Edison, L. K. et al. *Advances in microbial biotechnology: Current trends and future prospects* 53–72 (Apple Academic Press, 2018).
5. Zhou, Y. et al. A novel efficient beta-glucanase from a paddy soil microbial metagenome with versatile activities. *Biotechnol. Biofuels.* **9**, 36 (2016).
6. Han, B. et al. Gene cloning, expression and characterization analysis of a highly thermal stable β-glucanase gene from *Aspergillus niger*. *Food Ferment. Ind.* **44**, 55–62 (2018).
7. Hua, C. et al. Cloning and expression of the endo-1,3(4)-beta-glucanase gene from *Paecilomyces* sp. FLH30 and characterization of the recombinant enzyme. *Biosci. Biotechnol. Biochem.* **75**, 1807–1812 (2011).
8. Wang, X. et al. The atmospheric and room-temperature plasma (ARTP) method on the dextranase activity and structure. *Int. J. Biol. Macromol.* **70**, 284–291 (2014).
9. Li, J. et al. Purification and characterization of a new endo-β-1,3-glucanase exhibiting a high specificity for curdlan for production of β-1,3-glucan oligosaccharides. *Food Sci. Biotechnol.* **23**, 799–806 (2014).
10. Tasirnafas, M. et al. Extraction and purification of beta-glucanase from bovine rumen fungus *Trichoderma reesei* and its effect on performance, carcass characteristics, microbial flora, plasma biochemical parameters, and immunity in a local broiler hybrid Golpayegan-Ross. *Trop. Anim. Health Prod.* **52**, 1833–1843 (2020).
11. Wang, N. & Huo, Y. X. Using genome and transcriptome analysis to elucidate biosynthetic pathways. *Curr. Opin. Biotechnol.* **75**, 102708 (2022).
12. Prosser, G. A. et al. Metabolomic strategies for the identification of new enzyme functions and metabolic pathways. *EMBO Rep.* **15**, 657–669 (2014).
13. Chandrasekaran, V. et al. Evaluation of the impact of iPSC differentiation protocols on transcriptomic signatures. *Toxicol. In Vitro.* **98**, 105826 (2024).
14. Atanasova, L. et al. Comparative transcriptomics reveals different strategies of *Trichoderma mycoparasitism*. *BMC Genom.* **14**, 121 (2013).
15. Tian, Y. et al. Isolation and identification of Talaromyces sp. Strain Q2 and its biocontrol mechanisms involved in the control of Fusarium Wilt. *Front. Microbiol.* **12**, 724842 (2021).
16. Zhao, Y. et al. Transcriptome analysis of potential inhibitory mechanisms of *Talaromyces purpureogenus* Strain Q2 against *Fusarium oxysporum*. *Shandong Agric. Sci.* **53**, 94–101 (2021).
17. Nitsche, B. M. et al. The carbon starvation response of *Aspergillus niger* during submerged cultivation: Insights from the transcriptome and secretome. *BMC Genom.* **13**, 380 (2012).
18. Chappell, L. et al. Single-cell (Multi)omics technologies. *Annu. Rev. Genom. Hum. Genet.* **19**, 15–41 (2018).
19. de Oliveira, J. M. et al. Proteomic analysis of the secretory response of *Aspergillus niger* to D-maltose and D-xylose. *PLoS ONE* **6**, e20865 (2011).
20. Zhu, X. et al. Proteomics and metabolomics analysis of the lignin degradation mechanism of lignin-degrading fungus *Aspergillus fumigatus* G-13. *Anal. Methods* **15**, 1062–1076 (2023).
21. Xu, T.-L. et al. Yield enhancement of recombinant α-amylases in *Bacillus amyloliquefaciens* by ARTP mutagenesis-screening and medium optimization. *Sains Malays.* **48**, 965–974 (2019).
22. Gong, M. et al. Key metabolism pathways and regulatory mechanisms of high polysaccharide yielding in *Hericium erinaceus*. *BMC Genom.* **22**, 160 (2021).
23. Soga, T. et al. Quantitative metabolome analysis using capillary electrophoresis mass spectrometry. *J. Proteome Res.* **2**, 488–494 (2003).
24. Kohen, R. et al. Antioxidant activity of carnosine, homocarnosine, and anserine present in muscle and brain. *Proc. Natl. Acad. Sci. U.S.A.* **85**, 3175–3179 (1988).
25. Kavadia, A. et al. Lipid and γ-linolenic acid accumulation in strains of *Zygomycetes* growing on glucose. *J. Am. Oil Chem. Soc.* **78**, 341–346 (2001).
26. Beeharry, N. et al. Linoleic acid and antioxidants protect against DNA damage and apoptosis induced by palmitic acid. *Mutat. Res.* **530**, 27–33 (2003).
27. Marnett, L. J. & Plastaras, J. P. Endogenous DNA damage and mutation. *Trends Genet.* **17**, 214–221 (2001).
28. Ripps, H. & Shen, W. Review: Taurine: A "very essential" amino acid. *Mol. Vis.* **18**, 2673–2686 (2012).
29. Baliou, S. et al. Protective role of taurine against oxidative stress. *Mol. Med. Rep.* **24**, 15–41 (2021).
30. Toney, M. D. Controlling reaction specificity in pyridoxal phosphate enzymes. *Biochim. Biophys. Acta.* **1814**, 1407–1418 (2011).

31. Dong, M. et al. Integrative transcriptome and proteome analyses of *Trichoderma longibrachiatum* LC and its cellulase hyper-producing mutants generated by heavy ion mutagenesis reveal the key genes involved in cellulolytic enzymes regulation. *Biotechnol. Biofuels. Bioprod.* **15**, 63 (2022).
32. Borin, G. P. & Oliveira, J. V. C. Assessing the intracellular primary metabolic profile of *Trichoderma reesei* and *Aspergillus niger* grown on different carbon sources. *Front. Fungal Biol.* **3**, 998361 (2022).
33. Sun, M.-M. et al. Dihydrolipoamide acetyltransferase promotes nucleic acid synthesis by controlling phosphogluconate dehydrogenase acetylation. *Chin. J. Biochem Mol. Biol.* **37**, 339–346 (2021).
34. Chen, J. et al. *Determination of β-glucanase Activity in Feed Additives-Spectrophotometry*. (China Agric. Press, 2020).
35. Zelena, E. et al. Development of a robust and repeatable UPLC-MS method for the long-term metabolomic study of human serum. *Anal. Chem.* **81**, 1357–1364 (2009).
36. Kanehisa, M. & Goto, S. KEGG: kyoto encyclopedia of genes and genomes. *Nucleic Acids Res.* **28**, 27–30 (2000).
37. Kanehisa, M. et al. KEGG for taxonomy-based analysis of pathways and genomes. *Nucleic Acids Res.* **51**, D587–D592 (2023).
38. Kanehisa, M. Toward understanding the origin and evolution of cellular organisms. *Protein Sci.* **28**, 1947–1951 (2019).

Acknowledgements

This study was supported by the Technology R&D Plan for Key Areas of Xinjiang Production and Construction Corps (2022AB013) and the Project of Fund for Stable Support to Agricultural Sci-Tech Renovation (xjnky-wdzc-2023005-6).The authors would like to express their gratitude to Novegene Co. Ltd. (Beijing, China) for transcriptomic sequencing, and BioNovogene (Suzhou, China) for metabolomic analysis.

Author contributions

N.W. conducted the experiments, analyzed the data, and wrote the manuscript. Q.L. analyzed the data, developed the concept, and guided the experiment. Z.H.W. participated in the data analysis. H.L.S. participated in the experiments. Y.G. and J.Z. analyzed the data and revised the manuscript. K.L. and X.D.H. provided financial support, developed the study concept, guided the entire study process, and revised the manuscript. All the authors have read and approved the final manuscript for submission.

Declarations

Competing interests

The authors declare no competing interests.

Additional information

Supplementary Information The online version contains supplementary material available at https://doi.org/10.1038/s41598-025-07954-y.

Correspondence and requests for materials should be addressed to K.L. or X.H.